Journal of Electroceramics, 12, 69–88, 2004
© 2004 Kluwer Academic Publishers. Manufactured in The Netherlands.

# Non-Conventional Micro- and Nanopatterning Techniques for Electroceramics

M. ALEXE, C. HARNAGEA & D. HESSE*
*Max-Planck-Institut für Mikrostrukturphysik, Weinberg 2, D-06120 Halle, Germany*

**Abstract.** An overview of non-conventional methods being used for micro- and nanopatterning of electroceramics is given, including various top-down and bottom-up approaches. Within the top-down approach, focussed ion beam patterning, electron-beam direct writing, nanoimprint lithography, and other next-generation lithography techniques are considered, whereas several physical and chemical self-patterning routes are described for the bottom-up approach. Also included is a chapter on ferroelectric testing of nanopatterned electroceramics, with emphasis laid on possibilities and limitations of piezoresponse scanning force microscopy.

**Keywords:** nanopatterning, electroceramics, next generation lithography, self patterning, piezoresponse scanning force microscopy

## 1. Introduction

Many applications of electroceramics require micro- or even nanopatterning of a thin film. For example, piezoelectric micro-sensors and micro-actuators involve piezoelectric thin films patterned into structures of micrometer-range sizes. For high-density memory applications in integrated microelectronics, ferroelectric thin films patterned into nanometer-range sizes are required [1]. For example, in a prospective 10 Gbit non-volatile ferroelectric random access memory (NV-FeRAM), the lateral area of the whole memory cell, consisting of a capacitor and a transistor, should not exceed 100 nm, implying ferroelectric capacitors having lateral dimensions well below 100 nm.

Fundamental questions arise in this respect, e.g., whether electroceramic cells of 100 nm lateral sizes are still piezo- or ferroelectric, considering the well-known "collective" or correlated character of ferroelectricity [2]. Other questions are, whether and how the piezoelectric or ferroelectric properties of the thin films are influenced by the patterning process itself, and whether the relatively large proportion of surfaces and interfaces leads to domain pinning or to other surface- or size-related problems, see, e.g. [3–5]. For an experimental study of these questions, micro- and nanopatterning techniques for electroceramic materials are fundamental prerequisites. In the following, an overview of non-conventional methods for micro- and nanopatterning of electroceramics is given, together with a description of testing techniques required for investigations of micro- and nanopatterned electroceramics.

*To whom all correspondence should be addressed. E-mail: hesse@mpi-halle.de

## 2. Top-Down Approaches

### 2.1. Focussed Ion Beam Patterning

Focussed ion beam (FIB) patterning is nowadays used on rather large scale in the microelectronics industry to pattern structures with lateral sizes down to several tens of nanometers. The FIB equipment is conceptually similar to a scanning electron microscope (SEM), but instead of a beam of electrons, a highly focussed beam of gallium ions is used to scan the sample surface. This ion beam can be used for two purposes: imaging, and micromachining: Scanning a low-current beam over an area of the sample surface and simultaneously collecting the induced secondary

electrons, one can produce a high-resolution image of the sample, whereas at high beam current, high-precision local sputtering and milling can be easily performed. FIB equipment also allows the fabrication of small structures by direct deposition of metals (such as tungsten, gold, or platinum) or insulators (like silicon dioxide) with a minimum feature size down to 40 nm and a precision of 10 nm, allowing studies on quantum transport mechanisms [6]. Various materials can be selectively etched in reactive gas atmospheres achieving aspect ratios up to 30 with a minimum feature size below 25 nm. Having the unique nanopatterning ability to add or remove features with a resolution of 20 nm or better, the FIB method is currently used to modify integrated circuits and masks, or to fabricate cross section transmission electron microscopy specimens.

In the attempts of preparing switchable ferroelectric structures as small as possible, FIB patterning was among one of the first methods to nanofabricate ferroelectric capacitors with sizes down to sub-100 nm lateral size. Ganpule et al. fabricated ferroelectric capacitors made of $Pb(Zr,Ti)O_3$ (PZT) and $SrBi_2Ta_2O_9$ (SBT) by cutting them out from a complex film structure [7, 8]. For the PZT capacitors the starting complex heterostructure consisted of a sequence of Pt–LSCO–PNZT–LSCO–Pt layers deposited onto silicon. The polycrystalline $Pb(Nb_xZr_yTi_z)O_3$ (PNZT) layer of 160–210 nm thickness was prepared by sol-gel deposition, and a $La_{0.5}Sr_{0.5}CoO_3$ (LSCO) conducting barrier layer of about 100 nm thickness was deposited onto a bottom Pt layer by PLD. For the SBT-based capacitors the starting structure was $Pt/SrBi_2Ta_2O_9/Pt$.

Milling was performed using a Micrion FIB-2500 machine equipped with a liquid gallium ion source, operating at 50 kV accelerating voltage, 2–1500 pA beam current, and a corresponding beam diameter of about 6–100 nm. Scanning the beam within the chosen area was performed by a digital serpentine scan with a pixel dwell time of 1–50 ms and a distance of 10 nm between pixels, to provide sufficient overlap of the beam. The film heterostructures were milled down to the bottom conductive layer (which required the removal of up to 400–450 nm of material) in a designed pattern, viz. an island with the top Pt/LSCO layer forming one electrode (Fig. 1).

The advantage of this technique is the possibility of using an established method to produce high-quality thin films, including epitaxial films, such as PLD or MOCVD. This allows a comprehensive macroscopic characterisation of the film before nanopatterning, avoiding the potential compositional or structural deviations which might be involved in other nanofabrication techniques based on bottom-up approaches. FIB patterning has actually opened the possibility of direct comparisons between the properties of a patterned structure and the original film, establishing the large influence of in-plane clamping, induced by the substrate, onto the electromechanical properties of a ferroelectric film [9].

The major drawback of the method is associated with the high damage that occurs during milling and imaging, in particular, if a dual-beam FIB machine (where imaging is performed by a primary *electron* beam) is not available. While most of the structural defects can be healed by a high-temperature thermal annealing after milling, a gallium doping is basically unavoidable and in special cases might be relatively harmful to the final electrical properties. Detailed studies on radiation damage during the FIB process and its recovery were performed by Stanishevsky et al. [10]. They discovered that the exposure of a PZT film to a gallium ion beam of 50 kV dramatically changes the composition of a near-surface layer and leads to a more or less pronounced modification of the ferroelectric properties, depending on the radiation dose (Fig. 2). The modified near-surface layer is rich in gallium and depleted in oxygen. The gallium concentration is lower on the side walls due mostly to sputtering and shallower implantation. Gallium has a strong tendency to segregate into nanosize droplets during the milling and additionally might precipitate and diffuse along the grain boundaries of the film, creating local conducting channels and increasing the leakage current.

A thermal annealing of the cut-out structures recovers the ferroelectric properties, but in general a damaged layer up to 10 nm thick still remains, in which the ferroelectric properties are altered. Obvously, this would affect only structures with lateral sizes less that 100 nm. Despite this major drawback, the nanopatterning via FIB is an extremely versatile method that allows fabrication of diverse nanoscale ferroelectric systems starting from their film counterpart. Whereas FIB patterning is well suited to prepare single nanostructures, the preparation of cell arrays requires methods that are less time-consuming and have more of a parallel character. Among them are electron beam direct writing, nanoimprint lithography, and other next generation lithographies.

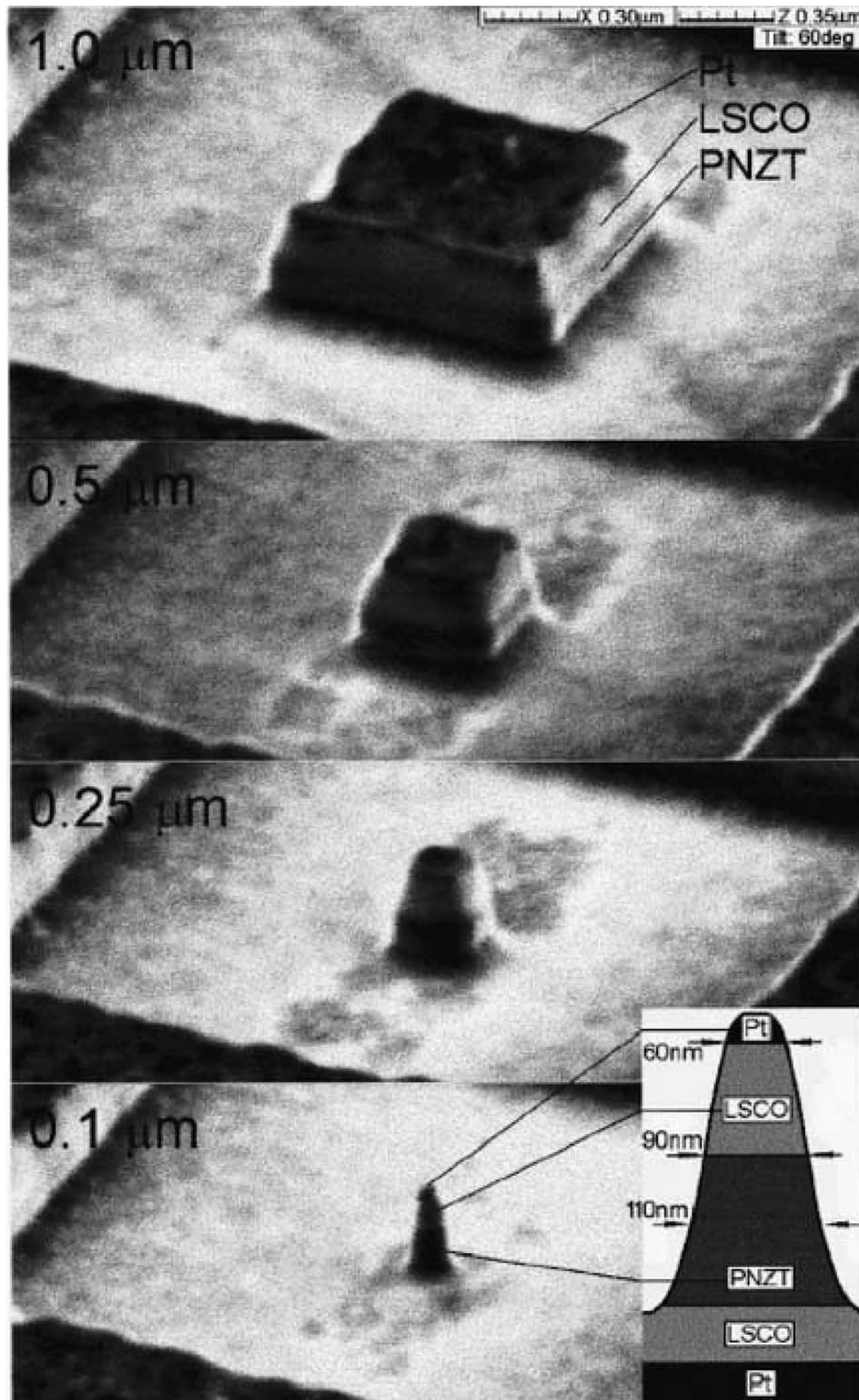


*Fig. 1.* Scanning ion-beam images of ferroelectric test structures fabricated by focussed ion-beam milling in the size range from $1 \times 1$ $\mu$m to $0.1 \times 0.1 \mu$m. The contrast from the various layers in the heterostructure is clearly visible. The inset is a schematic of the shape and dimensions of the 0.1 $\mu$m test structure. (After Ref. [7]).

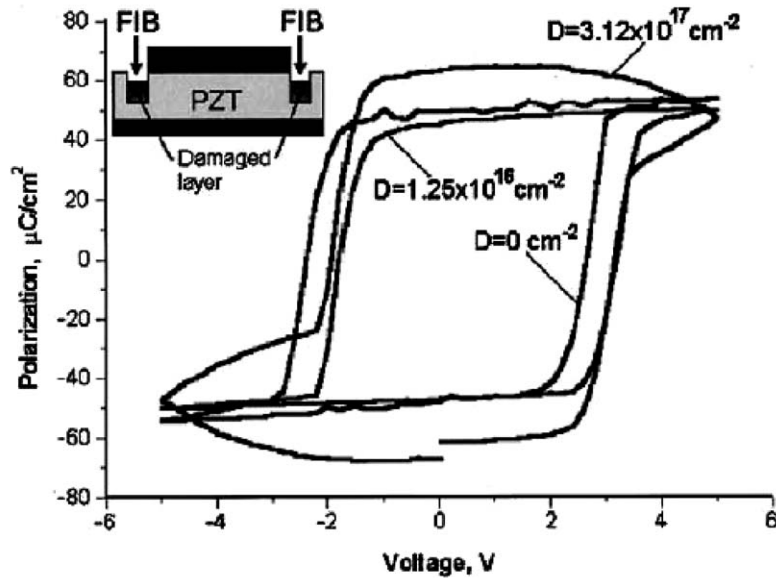


*Fig. 2.* Effect of the ion dose on the polarization hysteresis loops of FIB-patterned ferroelectric capacitors. (After Ref. [10]).

### 2.2. *Electron Beam Direct Writing*

At the end of the nineties, electron beam direct writing (EBDW)—prior applied to other materials [11, 12]—was first used to prepare ferroelectric arrays. Arrays from $Bi_4Ti_3O_{12}$ [13], $SrBi_2Ta_2O_9$ [14] and PZT [15], with individual cells of 150 nm [13] and 100 nm lateral size [14, 15], respectively, were prepared and shown to display ferroelectric properties. An electron-beam lithography approach using a PMMA film as resist, a chromium mask, and a dry etching process has recently been applied to this end as well, cf. [5].

As an example for EBDW, Fig. 3 shows scanning electron microscope (SEM) images of PZT arrays. Starting from a solution containing metalorganic compounds or metal colloids, a substrate is spin-coated with a thin precursor film that contains the required elements (various metals and oxygen) in a proportion corresponding to that of the later ferroelectric phase (Fig. 4). For example, precursor films for SBT and PZT structures can be prepared from Sr-, Bi-, and Pb-ethylhexanoate, Ti- and Zr-isopropylene, and Ta-methoxide solutions, using xylene and 2-methoxyethanole, respectively, as solvents. The obtained precursor film is then patterned by scanning an electron beam of, e.g., 3 nm diameter over selected areas of the film (“pattern exposure”), and immersing the exposed sample for 1 minute in toluene (“pattern development”), followed by dry-blowing with nitrogen. In our case, EBDW was performed using a commercial electron beam lithography system (ELPHY Plus, Raith Co.) adapted to a JEOL JSM SEM with $LaB_6$ cathode, working at 40 kV acceleration voltage. The electron doses used during exposure were from 600 to 1200 $\mu C/cm^2$ for SBT, and 1500 to 6000 $\mu C/cm^2$ for PZT, depending on film thickness and cell size. After pattern development, the still metalorganic mesas are transformed into an amorphous mixed oxide phase by low-temperature annealing in air, and subsequently the required ferroelectric phase is obtained by a high-temperature anneal in air. For example, the low-temperature anneal is performed at 300°C for 5 min, and the subsequent high-temperature anneal at 600 to 850°C for one hour. The two annealing processes lead to quite a shrinkage of the original mesas in size, of the order of 40 to 50% overall, and they may result in more or less pronounced shape changes, depending on the material. PZT mesas were observed to almost fully maintain their original shape, although shrinking in size by 50%.

The resulting crystalline patterns (cf. Fig. 3) consist of individual cells that are polycrystalline, implying very small grains with sizes of the order of 10 to 20 nm. As it was shown by piezoresponse scanning force microscopy (PFM; for a detailed description, see Section 4.2), the cells respond to a d.c. field with a

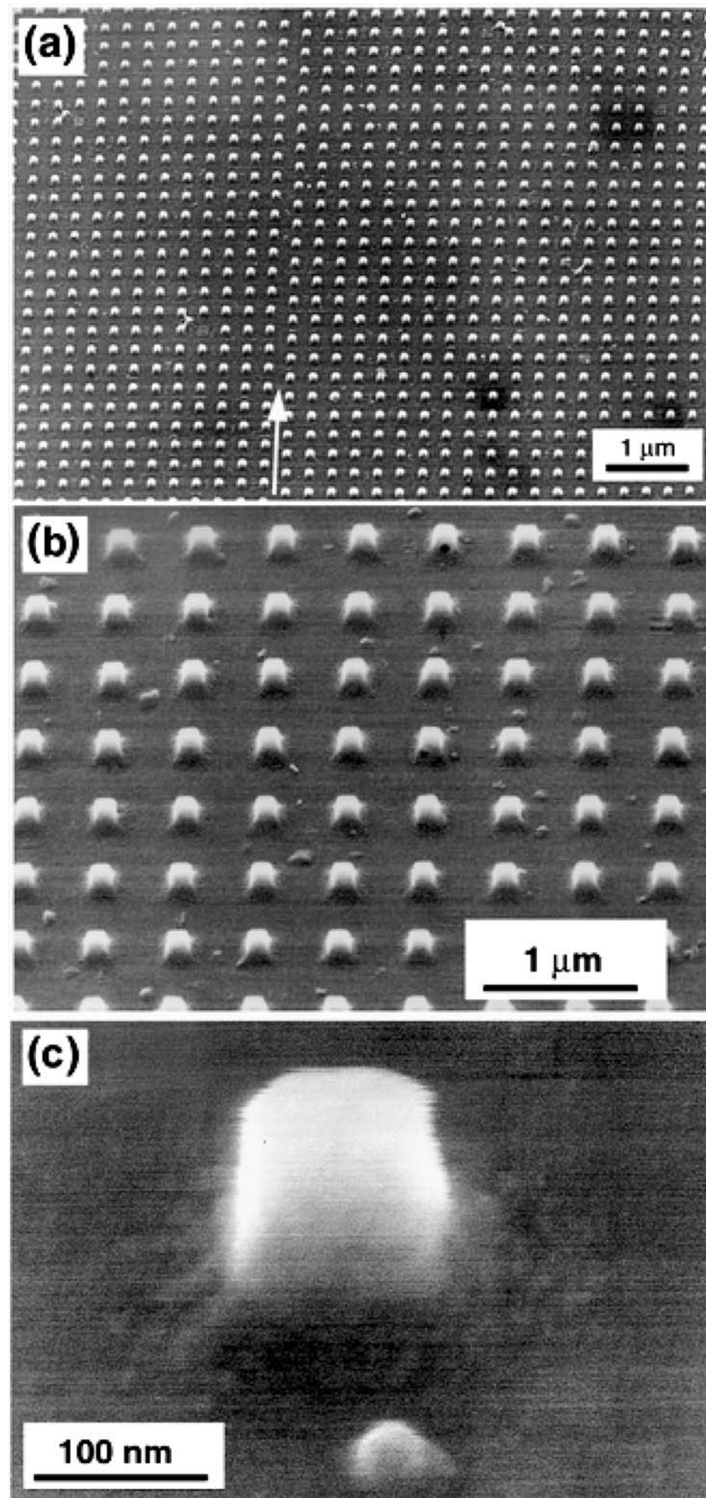


*Fig. 3*. (a) Scanning electron micrograph of an array of PZT cells with 100 nm lateral size prepared by EBDW. The array contains a purposely introduced antiphase boundary (see arrow). (b) and (c) Differently magnified images of this array.

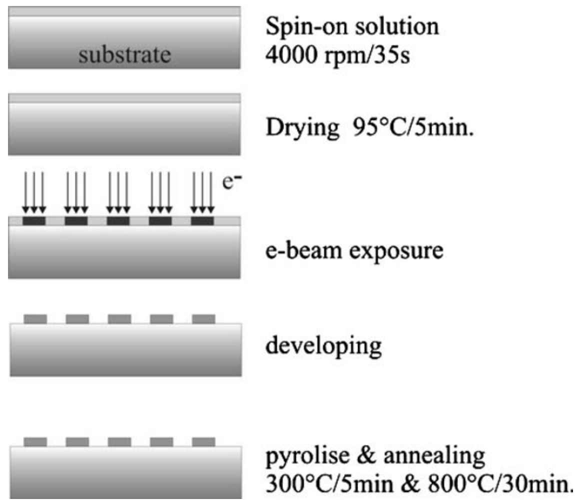


*Fig. 4*. Process flow chart of electron-beam direct writing of ferroelectric cell arrays.

piezoelectric hysteresis loop, which clearly shows that they are ferroelectric [16]. Figure 5 presents such hysteresis loops, one for a cell of 1 $\mu$m lateral size, the other for one of 100 nm lateral size. From investigations of this kind it became clear that PZT cells $100 \times 100 \times 100$ nm$^3$ in size still display ferroelectric properties. As the interaction between the tip of the scanning force microscope (SFM) and the sample is very complex [17–19], neither the absolute polarisation values nor the true coercive field can be deduced from these measurements.

The cells obtained in this way were used to study switching and size effects using PFM [14, 20]. In PFM images, white and dark contrasts are associated with the two remanent polarisation states $\pm P_r$, and a grey contrast indicates the absence of out-of-plane piezoresponse. In-plane investigations, probing the in-plane components of $P_r$, are possible as well, cf. Chapt. 4.2.

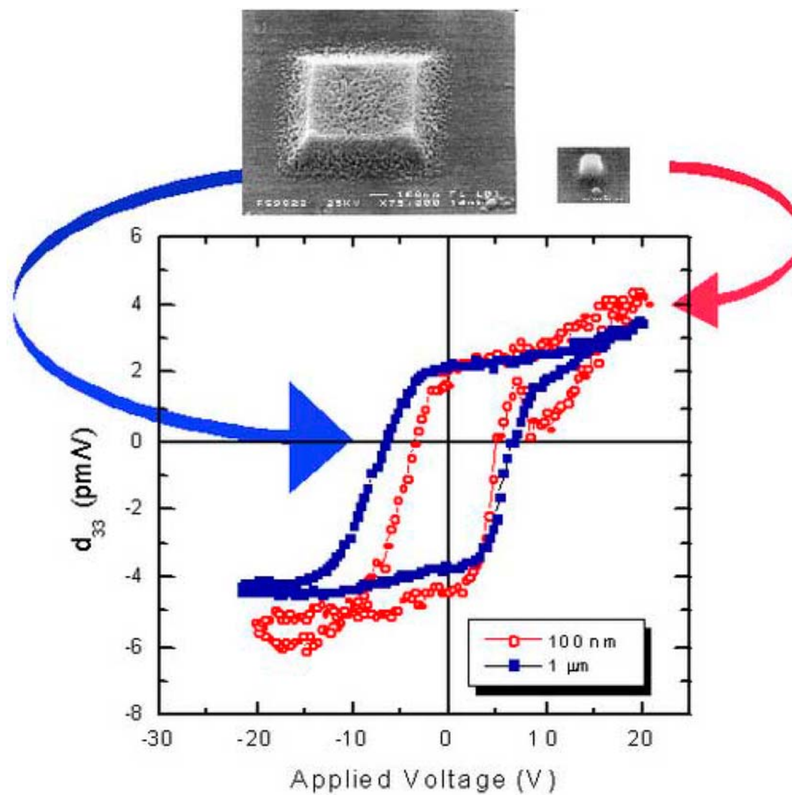


*Fig. 5*. Piezoelectric hysteresis curves of two PZT cells prepared by EBDW, one with 1 $\mu$m lateral size, the other with 100 nm lateral size. Insets: SEM micrographs of the two PZT cells.

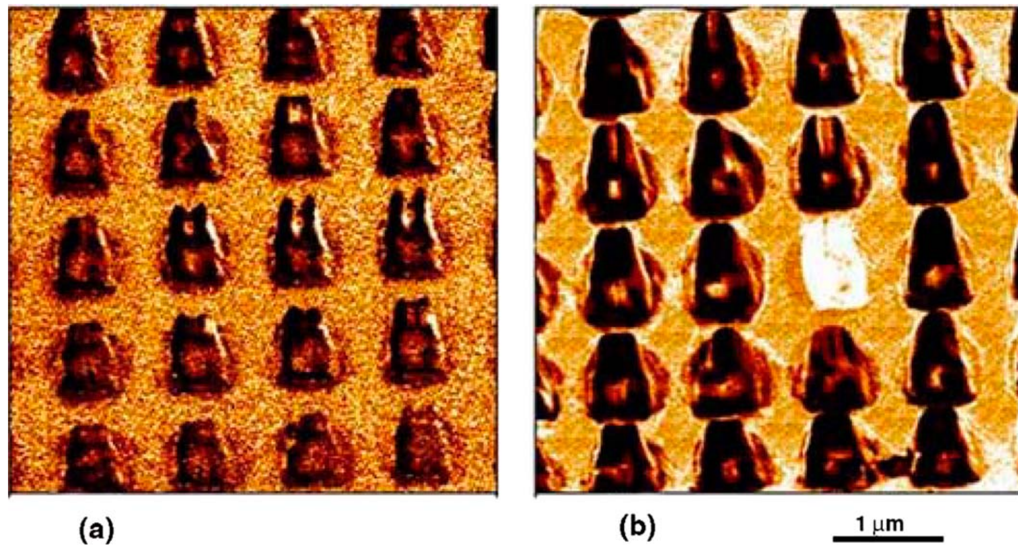


*Fig. 6.* PFM images of a PZT cell array prepared by EBDW, with cells of 250 nm lateral size., viz. (a) before, and (b) after switching a cell with a +20 V pulse. Note the switching of the entire cell volumes and the absence of cross-talk.

Figure 6 shows a PZT array consisting of cells with a lateral size of 250 nm. The entire array was first uniformly poled into a negative state (black colour) with a −20 V pulse (Fig. 6(a)), before then switching one selected cell into the positive state (white colour) applying a +20 V pulse to this cell (Fig. 6(b)). Due to the convolution with the tip shape, the shape of the cells appears distorted in Fig. 6. During switching, no cross-talk occurred, as is also obvious from Fig. 6(b).

Detailed investigations of this kind proved the existence of imprint and size effects in PZT cells with lateral sizes between 1 $\mu$m and 75 nm [20]. It turned out that the free lateral surfaces of the cells "pin" a layer of about 35 nm thickness, preventing the switching of the near-surface volume of the cell. This layer may prevent the application of EBDW-prepared PZT cells with a lateral size below 70 nm, if this application requires switching. In addition, indications of a ∼10 nm thick layer close to the bottom electrode were obtained, which does not switch. This layer may represent a depletion layer [21, 22], or rather the high-density oxygen vacancy layer associated with domain pinning in the fatigue model of Scott and Dawber [23].

Overall, electron-beam direct writing proved a powerful method to prepare arrays of ferroelectric cells with lateral sizes down to 75 nm, although with quite an effort of expensive equipment and time. It is therefore rather suited for research purposes than for industrial mass production. For the latter, more economic means of preparation have to be developed.

### 2.3. *Nanoimprint Lithography*

A method to prepare ferroelectric cell arrays that is potientially suitable for industrial mass production, is nanoimprint lithography (NIL). Traditional NIL has emerged as a rapid, low-cost technique for the preparation of nanostructures in polymer films like PMMA with structure sizes well below the limit of other lithography techniques, down to 20 nm feature size [24–26]. Similar to imprint into polymer films, we have proposed the use of NIL to obtain large arrays of ferroelectric cells. Using a variant of this technique, we succeeded in preparing arrays of ferroelectric cells with lateral sizes down to 250 nm so far, and we proved the ferroelectric nature of these cells using PFM [27].

The standard NIL technique implies the use of a thermoplastic resist which becomes a viscous liquid above its glass transition temperature and which thus can flow above this temperature. Thus it can be deformed easily. NIL is usually performed in two steps. In the imprint step, a mold with the negative of the desired pattern on its surface is pressed into a thin resist cast on a substrate, followed by removal of the mold. This step transfers the pattern of the mold into the resist film, or,

in other words, it creates a thickness contrast pattern in the resist. The second step is the pattern transfer in which an anisotropic etch process, such as reactive ion etching (RIE), is used to remove the residual resist in the compressed area. This step transfers the thickness contrast pattern into the entire resist. Preparing ferroelectric arrays begins with spin-coating a substrate with a precursor film, most similar to the first step of EBDW. This precursor film is prepared by a chemical solution deposition (CSD) technique. Subsequently, a thickness contrast is created in this precusor film by pressing a mold with a defined pattern into it. After removing the mold, the precursor is transformed into a ferroelectric by drying and annealing (Fig. 7).

Two chemical routes were explored for preparation of ferroelectric PZT cell arrays on conductive substrates, viz. Pt-coated silicon (Pt/Si) or Nb-doped $SrTiO_3$ (STO) serving as the bottom electrode: metalorganic deposition (MOD) and sol-gel deposition. In the MOD route, precursor solutions were spun onto the subtrates, forming thin films of thicknesses between 200 and 700 nm, depending on solution concentration and rotation speed. These precursor films were dried by annealing at 70°C, before they were imprinted. After imprint, the mesas were converted into the oxide by heating at 300°C, and finally crystallised into PZT by annealing at 650°C for 1 h. The sol-gel route was identical to the MOD route, except for the drying before the imprint step. An optimum imprint pressure of 1 kbar was applied using a laboratory press at room temperature. The molds used consisted either of macroporous silicon, prepared by electrochemical methods [28], or of $SiO_2$-covered silicon wafers patterned by photolithography and reactive ion etching. The smallest size of the negative features in the mold (holes, pores) was ca. 400 nm for porous silicon and 2 $\mu$m for the $SiO_2$/Si molds.

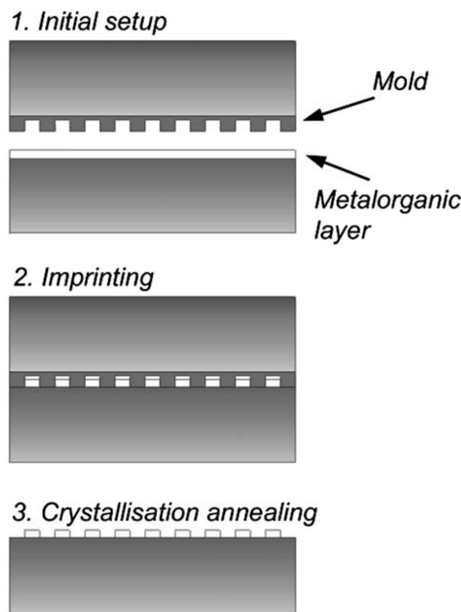


*Fig. 7.* Process flow chart of the preparation of ferroelectric cell arrays by nanoimprint lithography.

An important question is whether the shape of the imprinted pattern is maintained during crystallisation. For maintaining the shape, the size of the grains formed after annealing has to be well below the feature size of the pattern, at least by one order of magnitude. Figure 8(a) compares the grain size distributions of the ferroelectric films obtained on STO substrates using the MOD and sol-gel techniques. The maximum for MOD is at 240 nm, while that for the sol-gel route is at 35 nm. This explains why the size of the smallest structures we could obtain using MOD, without losing the shape of the structure, was 1.25 $\mu$m. The sol-gel method is most suitable for achieving structures with a lateral size in the 100 nm range, while still preserving the shape of the mold. A typical Si mold of 500 nm pitch is shown in Fig. 8(b). The diameter of the pores is 350–450 nm while the walls are 50–150 nm thick. The cells obtained using such a mold and the sol-gel route are shown in Fig. 8(c). The shape of the mold is well preserved due to the small grain size after crystallisation. The cells have an apparent diameter of 350 nm (full width at half maximum) and an average height of 50 nm, as shown by the cross-section profile in Fig. 6(d). Using tip-deconvolution software packages we found the lateral size to be even smaller by some 50 to 80 nm, i.e. in the 250–300 nm range. The images in Figs. 8(e) and (f) are the topography and the corresponding PFM image of a sample prepared by MOD. The topographic image shows that the sizes of the grains formed is too large to preserve the shape of the mold after crystallisation. The PFM image reveals that the cells are not entirely crystallised. The flat grey areas representing the complete absence of piezoresponse show that there is no component of the spontaneous polarisation out of the substrate plane. An attempt to orient the polarisation out of the substrate plane failed. In contrast, nice hysteresis loops were obtained from the region showing strong (bright or dark) contrast. From all these findings it is clear that the sol-gel route is more suitable for the

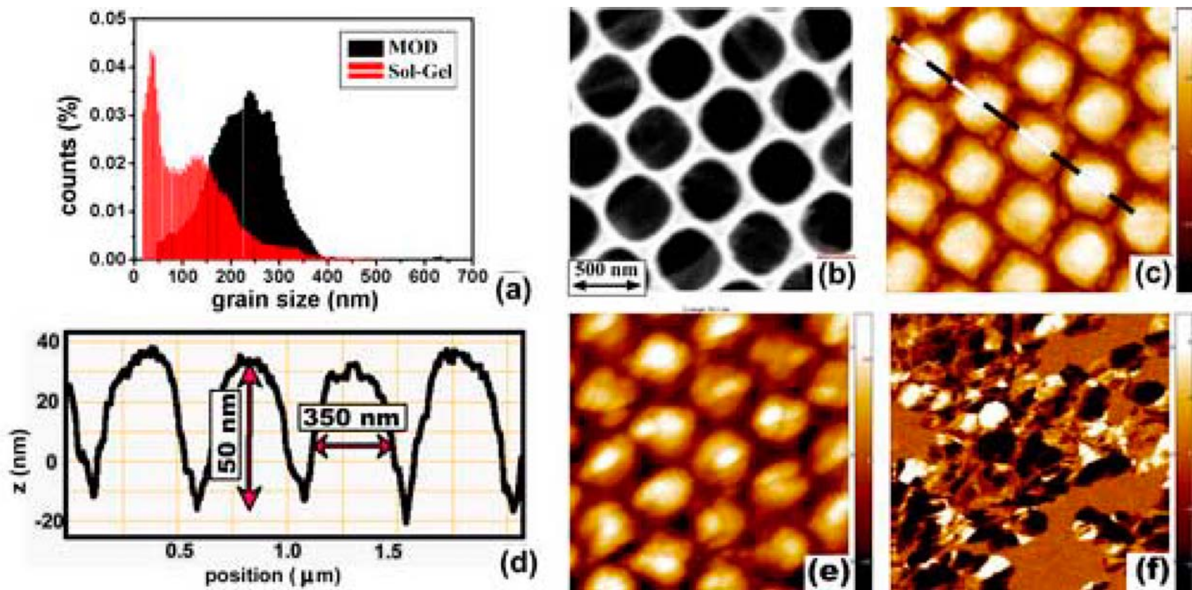


*Fig. 8.* (a) Grain size distribution of continuous ferroelectric films obtained on STO substrates using the MOD and sol-gel technique, respectively. (b) Macroporous silicon with an interpore distance of 500 nm, i.e. ca. 400 nm pore diameter. (c) Topographic image of the cells obtained by imprinting a sol-gel film using the mold shown in (b). (d) Cross-section line scan of (c) along the marked dashed line. (e) Topography image of the cells obtained using MOD and the mold shown in (b). (f) Piezoresponse image of the area corresponding to (e).

fabrication of ferroelectric cells, since the shape of the cells is well preserved down to a size of about 250 nm, and the cells are entirely crystallised (not shown here). The sol-gel solution, however, is sticky and often adheres to the mold. To overcome this problem, the mold should be coated with an inert anti-sticking layer to reduce the adhesion between gel and mold.

The functionality of the ferroelectric cells obtained—using the sol-gel method for the film deposition prior to imprint—is demonstrated in Fig. 9. Selected cells were poled by applying pulses of 15 V to the scanning probe microscope tip for a time of 3 s. The lateral size of the switched areas is around 200 nm, a size that is most probably due to the large radius of the tip apex. This is also suggested by the fact that the switched areas do not take the shape of the ferroelectric cell, but they are rather circular. The switched areas were stable at the time scale of the experiment: For at least three days no backswitching and no crosstalk occurred. Several aspects of the preparation of ferroelectric cell arrays by NIL still need further consideration, see Ref. [27]. However, we believe that it should be possible to achieve large-area, low-cost ferroelectric cells below 100 nm in lateral size with good ferroelectric properties using nanoimprint lithography.

### 2.4. *Next Generation Lithography*

Conventional photolithography is based on the old principle of photography, in which a negative is used to multiply an image (the positive pattern) as many times as necessary. The negative is called mask and the pattern (positive image) is transferred into some special photosensitive polymeric material, the photoresist, that after patterning acts as a mask for either an etch or a lift-off process. The intrinsic limit of this exceptionally simple and productive method is connected to the wavelength of the light used to transfer the mask pattern into the photoresist. Modern photolithography techniques can create features of about 100 nm in mass production and about 70 nm in experimental setups.

To improve the resolution of the above process up to several tens of nanometers would require the use of an electromagnetic radiation with a smaller wavelength, such as either extreme ultraviolet light with wavelengths between 10 and 70 nm, or X-rays with wavelengths between 0.1 and 10 nm. The high costs of such lithography tools, that could exceed the annual budget of a University or a research center, has initiated the emergence of a research field in which the aim is to establish simple and inexpensive nanofabrication methods. Along with nanoimprint lithography

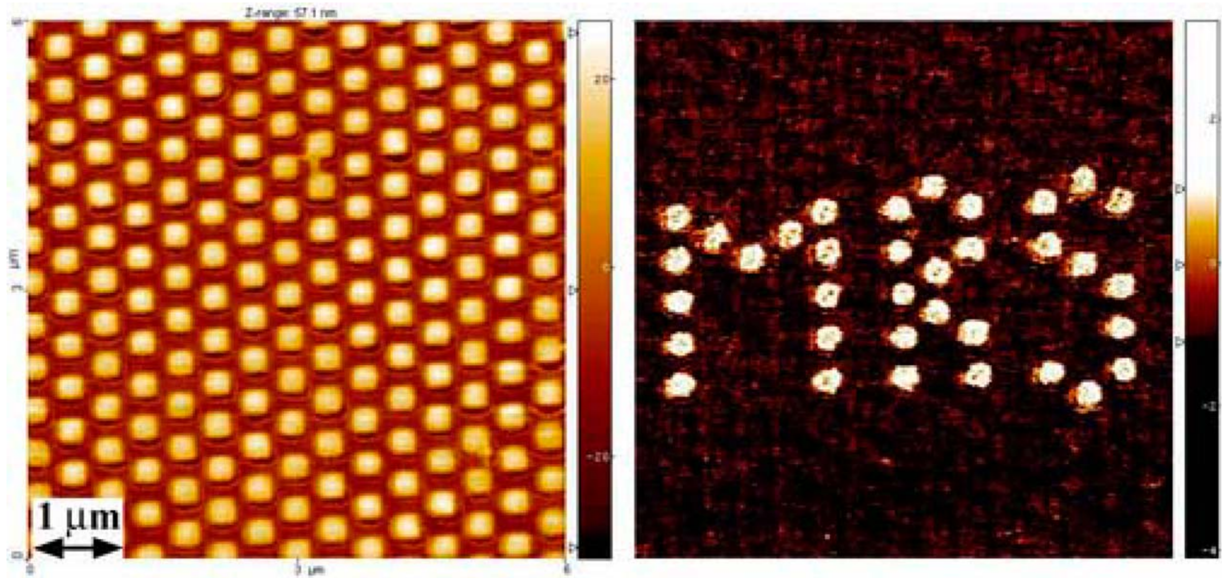


*Fig. 9.* Topography image of an array of ferroelectric PZT cells on STO substrate (left) and piezoresponse image of the same array (at the same magnification) after switching several cells using d.c. pulses applied to the tip (right).

described previously, two other methods based on stamps have been developed, viz. microcontact printing and micromolding in capillaries. Both have been recently developed by the Whitesides group at Harvard University [29, 30]. These methods, also called soft lithography methods, are based on the fabrication of soft molds or stamps using a soft rubbery polymer (polydimethylsiloxane-PDMS). In a first step, a master mask is fabricated on a substrate of choice, e.g. silicon, using conventional photo- or e-beam lithography. Then stamps are fabricated by replication of the master hard mask by simply pouring PDMS and subsequently curing it. The stamp can then be used in two modes. One mode is microcontact printing, in which the stamp is covered by a special solution containing molecules known to form self-assembled monolayers (SAMs), for instance thiol molecules on gold. When the stamp is brought into contact with the sample surface, the desired pattern of SAMs is transferred. In the second mode, the micromolding technique, the stamp is placed on a hard surface and a liquid polymer flows by capillary forces into the free space between the mold and the surface. While microcontact printing has a relatively poor resolution of only few microns, micromolding can replicate structures smaller than 10 nm.

Although the soft lithography is not an appropriate method for microelectronics, several advantages over the classical photolithography can be enumerated. Soft lithography methods are extremely useful in the case of patterning on non-flat surfaces, are relatively tolerant against a dusty environment, are cheap and can be used in combination with a wide range of materials, ferroelectrics being among the most interesting ones.

There is only a very small number of reports in literature on patterning ferroelectrics by combining soft lithography and chemical solution deposition methods such as sol-gel or metaloganic decomposition. Microcontact printing has been used together with sol-gel processing to selectively deposit oxide thin films with micron-scale lateral resolution. Patterned structures, such as capacitors and waveguides, have been fabricated from $LiNbO_3$, $PbTiO_3$, and $BaTiO_3$ on different substrates, including Si, Al, Pt, sapphire, and TiN. The technique involved functionalisation of substrate surfaces by microcontact printing of octadecyltrichlorosilane (OTS) self-assembled monolayers (SAMs). Sol-gel precursors are then spin-coated on the SAMs-patterned surfaces and heat-treated to deposit amorphous oxide layers of a thickness between 20 and 300 nm. The oxide on the functionalised regions is removed with mild polishing, yielding patterned films with features as small as 5 $\mu$m [31].

Micromolding has found a niche in MEMS technology, particularly in patterning of micron-scale

piezoelectric structures [32, 33]. Ceramic thick film and usual photolithography technologies have been used to develop micromolding of PZT thick films with lateral features down to 10 $\mu$m and aspect ratios up to 7:1 using soft reusable polydimethylsiloxane (PDMS) molds in order to fabricate piezoelectric actuators and transducers [34].

Dip-pen nano-lithography, developed by Mirkin of Northwestern University, is a method based on "literarily" writing patterns with an AFM tip and using a special ink that usually is based on thiol molecules, as in the microcontact printing [35]. Although the method has not yet been applied to pattern ferroelectric nanosize structures, it is obvious that dip-pen lithography has a certain potential in the field of fabrication of nanoscale ferroelectrics. If an appropriate stable precursor "ink" would be developed to replace the thiol-based ink, features of several tens of nanometers across can be easily written. Nonetheless, the main disadvantage remains the serial processing and the specific instability of the precursor solution against hydrolysis.

## 3. Bottom-Up Approaches

All lithography-based patterning techniques described above are top-down approaches and represent the basis of nowadays microelectronics technology. They are very well suited to fabricate structures with extremely good spatial resolution and positioning precision, but are intrinsically limited to structures, the sizes of which are well above the lowest nanometer-scale sizes. Therefore, there is a considerable interest in other fabrication methods that are not based on carving thin films, but rather on building structures from the bottom using atoms and molecules. These bottom-up methods will in principle allow the inexpensive fabrication of structures with sizes of 10–20 nm in a parallel approach. The primary disadvantage of the bottom-up methods is the random positioning of the obtained nanostructures that will make a precise interconnection of them virtually impossible. Successful strategies and routes have been developed to synthesize nanoscale materials of numerous simple systems such as semiconductors (Si, CdS, InAs/GaAs) or metals. Complex systems such as ferroelectric oxides or any muticomponent oxides belonging to the class of functional materials have not yet been systematically addressed, despite the possibility of discovering new materials with unique properties.

Recently the first attempts to prepare ferroelectric nanostructures *via* bottom-up approaches have been published. The approaches can already be classified into two main routes, viz. physical and chemical, which are obviously based on different principles. Both routes will be briefly described in the following.

### *3.1. Self-Pattering via Physical Routes*

In the quest for smaller and smaller ferroelectric structures, the physical routes have proven simple and reliable, making use of simple physical processes. Well-known physical growth concepts, such as island growth, have already been successfully applied to grow nanosize dots of germanium on silicon, or of InAs on GaAs. An important role is played by the lattice constant mismatch between the substrate and the deposited film. Depositing an epitaxial thin film onto a single-crystal substrate with high lattice mismatch, the initial stages of the growth process are characterised by either the island (Volmer-Weber) or layer-than-island (Stranski-Krastanov) growth modes. In contrast to the layer-by-layer (Frank-van der Merwe) growth mode, which results in a smooth uniform film, the two former growth modes are suitable to grow crystalline nanosize dots. The effect is well known and has been carefully studied in the case of simple systems such as germanium on silicon [36], and has even found application in the growth of compound semiconductor lasers [37]. Only recently the same concept has been applied to the growth of complex oxide islands on different substrates, demonstrating ferroelectricity in PZT islands as small as 70 nm wide and 30 nm high [38, 39].

Pulsed laser deposition (PLD) and pulsed laser ablation are also potential methods to obtain nanoparticles deposited on a substrate or in the form of a dispersed powder, respectively. Pulsed laser ablation has been used to produce PZT nanoparticles with a relatively narrow size distribution. The experimental setup is rather complex and consists of a laser ablation chamber, a charger, and a furnace [40]. Single crystalline nanoparticles with an average diameter of about 7 nm and a standard deviation of 5.4% have been obtained. Visinoiu et al. have grown $BaTiO_3$ nanoparticles on $SrTiO_3$ substrates by a simple PLD process [41]. Using vicinal $SrTiO_3$ substrates, a certain degree of registration and self-organisation could be induced as shown in Fig. 10.

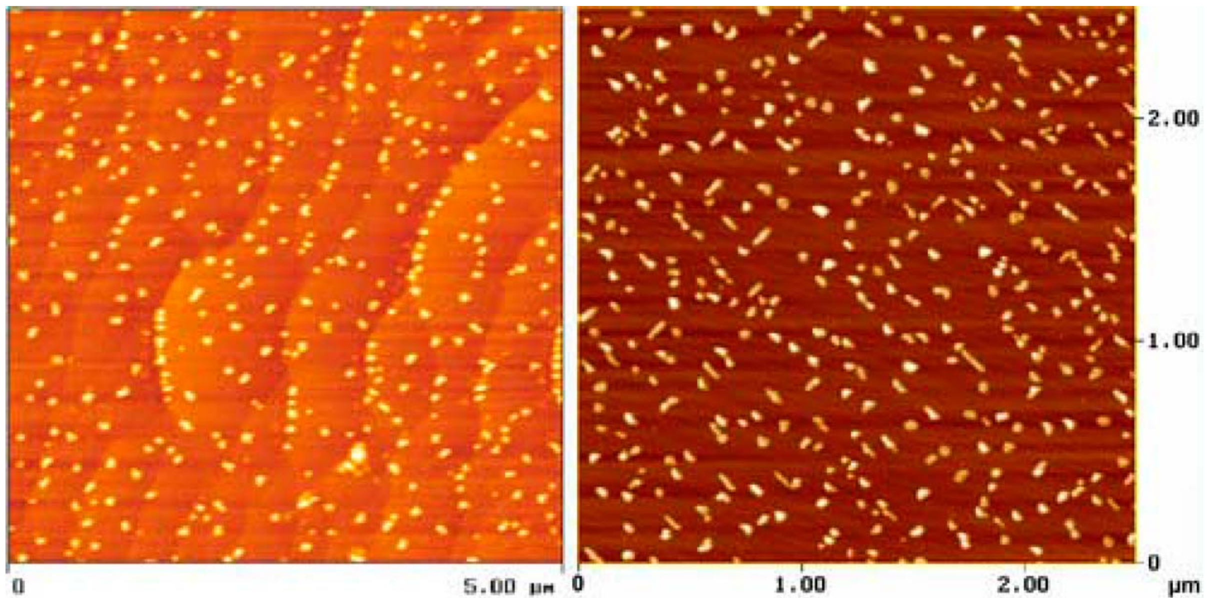


*Fig. 10.* SFM topography images of $BaTiO_3$ nanostructures deposited by pulsed laser deposition onto vicinal $SrTiO_3$(100) single-crystal surfaces.

Another method used to fabricate nanostructures is based on the concept of structural and morphological instability of ultrathin films. This possibility has been found during an effort of growing single-crystal epitaxial films by chemical solution deposition (CSD). Lange, Speck, and coworkers have theoretically and experimentally established that an ultrathin amorphous layer of PZT (or another perovskite oxide) deposited onto a single-crystal substrate such as $SrTiO_3$, during high-temperature crystallisation breaks up into small islands due to a microstructural instability [42]. The driving force of this process is the minimisation of the free energy of the film-substrate system, by lowering the interface area (forming islands) and by forming low-energy surfaces *via* faceting [43].

Polycrystalline nanosize structures have been fabricated by depositing ultrathin lead titanate ($PbTiO_3$) films onto Pt-coated silicon substrates using CSD. As a result of the high-temperature crystallisation by rapid thermal annealing, the deposited amorphous film breaks up into randomly oriented nanosize crystals with sizes ranging from 10 to 100 nm [44]. Using piezoresponse SFM, Roelofs et al. have shown that grains with lateral sizes of about 20 nm do not display an out-of-plane piezoelectric signal, suggesting that the size at which ferroelectricity vanishes in $PbTiO_3$ is about this size of 20 nm [45].

The main drawback of this experiment is the polycrystalline nature, i.e. the random orientation of the obtained grains. Without knowing the exact orientation of the measured crystallite it is extremely difficult to correctly interpret the piezoresponse signal [18], cf. Chapt. 4.2 below. Therefore it would be advantageous, at least in principle, to obtain epitaxial nanostructures rather than polycrystalline grains, so that the crystal orientation of all the epitaxial structures will be known. Szafraniak et al. have fabricated nanosize epitaxial PZT crystals using the microstructural instability method, Fig. 11 [46]. Structures with lateral dimensions of 40–90 nm have been obtained by conventional annealing of ultrathin amorphous oxide films at temperatures ranging from 800 to 1100°C. The size, shape and distribution of the nanocrystals could be tuned to some extent by modifying the initial film thickness and the crystallisation temperature (cf. Figure). The epitaxial nature of the crystals is revealed both by X-ray diffraction analysis and high resolution TEM investigations (Fig. 12). The ferroelectric properties of the individual islands were determined by piezoresponse SFM. There were no direct correlations between the lateral size of the structures and the presence of the piezoelectric activity. Well-developed hysteresis loops were acquired on structures either with large lateral size or with high thickness, suggesting that the piezoelectric activity is

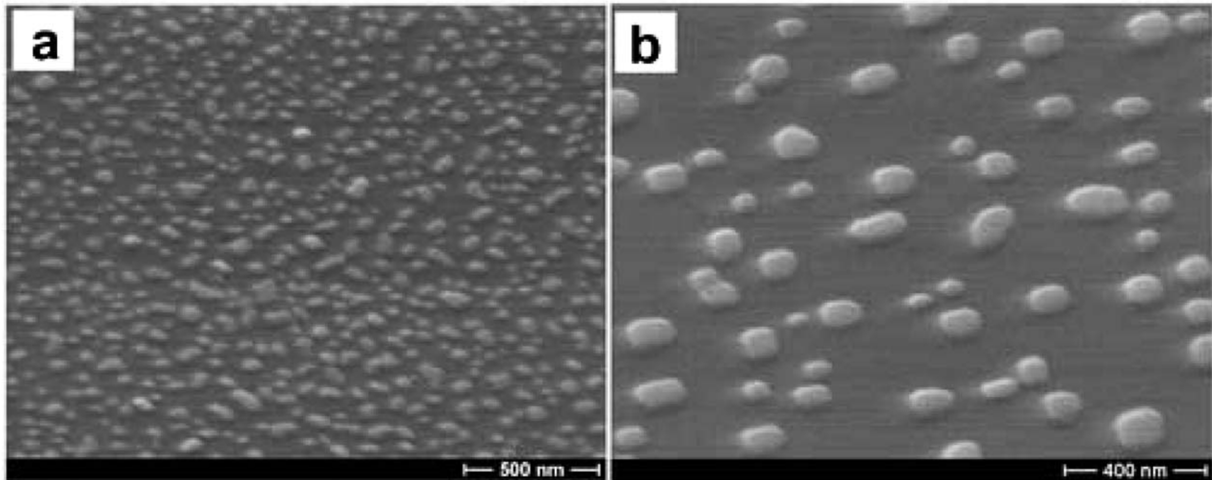


*Fig. 11.* Scanning electron micrographs of PZT nanocrystals crystallized at (a) 800°C and (b) 1100°C.

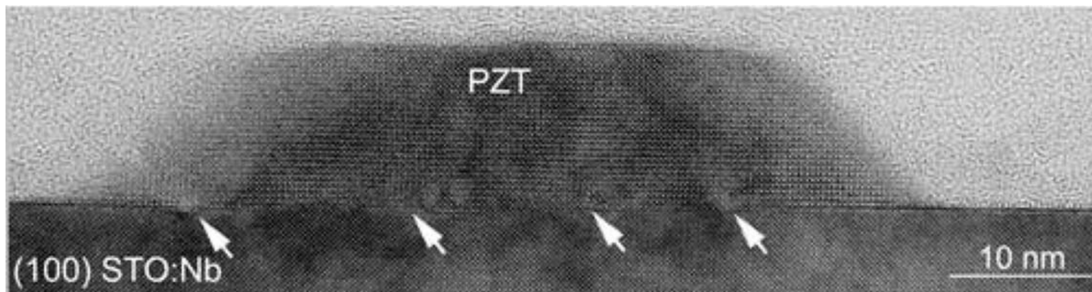


*Fig. 12.* High-resolution cross-section transmission electron micrograph of a small epitaxial PZT island grown on a $SrTiO_3$ single-crystal substrate. Arrows point to misfit dislocations.

connected rather to the volume of the structure than simply to the lateral size.

### *3.2. Self-Pattering via Chemical Routes*

A number of interesting fabrication approaches appear to be based on chemical routes. Using simple chemical routes it is possible to fabricate nanosize crystals or nanoparticles in colloidal suspensions, which can later be spread onto any substrate surface. After solvent evaporation the nanoparticles can be crystallised in two- or even three-dimensional arrays. Although obtaining a regular array of particles is not a simple and easy task, self-assembly concepts based on the reduction of the interfacial energy at the fluid-solid or fluid-fluid interface—concepts that have proven valid for more simple systems such as CdS [47]—can be used for more complicated systems such as ferroelectric oxides. In any case, one has first to develop methods to fabricate nanoscale ferroelectric particles. One of the most promising routes is based on the microemulsion concept in which a water-in-oil emulsion is produced using a surfactant. Such an emulsion consists of nanometer-size water droplets uniformly dispersed in an oily solvent. This microemulsion can be used to hydrolyse a complex metalorganic precursor. The nanodroplets act as nano-reactors in which the hydrolysis of the precursors takes place and, if the optimum conditions are fulfilled, the final reaction product consists of mono-dispersed nanosize particles [48].

A cyclohexane/Brij 30 (Polyethylene glycol dodecyl ether)/$H_2O$ water-in-oil microemulsion was used to hydrolyse a metallic alkoxide precursor (e.g., barium titanium ethylhexano-isopropoxide for $BaTiO_3$ particles) [49]. By adding the microemulsion to an

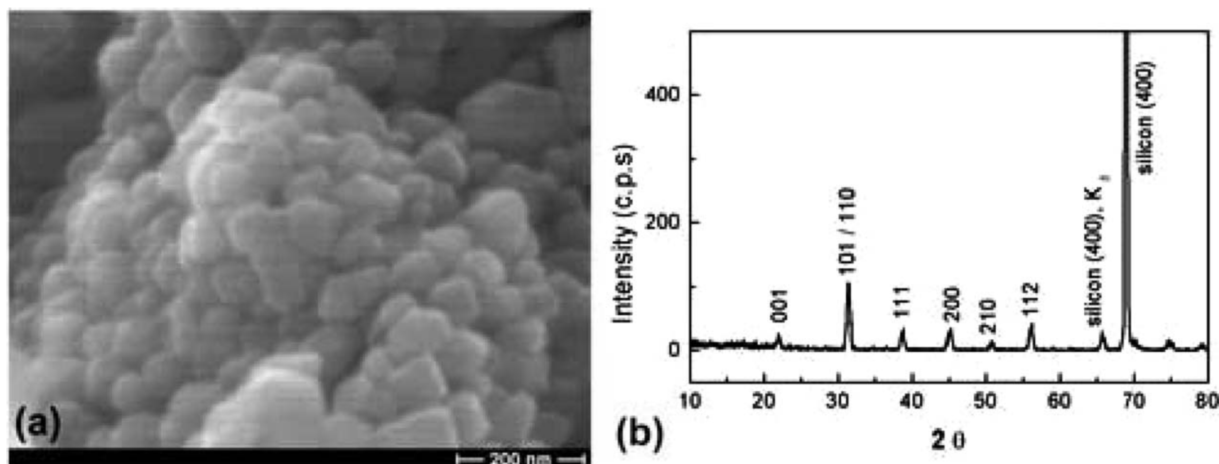


*Fig. 13.* (a) Microemulsion-derived $BaTiO_3$ nanopowder annealed at 450°C for 1 h, and (b) a corresponding XRD analysis showing the formation of single-phase $BaTiO_3$ nanopowder.

appropriate amount of bimetallic precursor, the latter reacts with the water droplets present in the microemulsion and forms oxide particles. After one hour of thermal treatment at 450°C, fully crystallised, single-phase $BaTiO_3$ nanosize powders are obtained (Fig. 13). To avoid agglomeration of the nano particles, tetrabutylammonium hydroxide can be used as a peptising agent.

A slightly different route to prepare nanosize $BaTiO_3$ was implemented by O'Brian et al. [50]. A single bimetallic alkoxide precursor (barium titanium ethylhexano-isopropoxide) is injected into a mixture of diphenyl ether and oleic acid as a stabilising agent at 140°C under inert atmosphere. After distillation of 2-propanol, the resulting solution is cooled to 100°C, and hydrogen peroxide is injected. The solution is maintained at this temperature for 48 h to promote hydrolysis and crystallisation, in the given inverse micelle (microemulsion) conditions. Monodispersed $BaTiO_3$ particles of 4 to 8 nm diameter are obtained. The diameter could be tuned by modifying the ratio between the alkoxide precursor and the oleic acid, which also passivates the particle surface, preventing agglomeration and enabling the transfer of the particles into a nonpolar solvent.

Concerning this route, two remarks are worth mentioning. First, the crystalline phase occurs at temperatures as low as 100°C, directly from the reaction. This is the only known route to obtain phase-pure perovskite oxides at such a low temperature. Second, at a more general level, the above route involving reactions in a so called inverse micelle, or colloidal-type solution (microemulsion route) is a generic route to synthesize nanoparticles. Due to its simplicity, its excellent output, and its low cost it might have an important impact in nanofabrication of ferroelectrics.

## 4. Ferroelectric Testing of Nanopatterned Electroceramics

Due to their small size, the characterisation of the cells or structures obtained cannot be achieved using conventional measurement techniques. For this purpose, scanning probe techniques, in particular scanning force microscopy (SFM), have proven to be most valuable. The principle of an SFM is quite simple [51]: A sharp tip mounted on a cantilever is brought close to a sample surface. The (attractive or repulsive) force between the tip and the surface is detected using the bending of the cantilever. A feedback loop adjusts the z-position of the cantilever using a piezoelectric element, so that the interaction force is kept constant. By scanning the tip over the surface and recording the z-position of the cantilever, a map of the sample topography can be obtained.[1]

Of particular interest in the characterisation of electroceramic materials is the use of a conductive SFM tip as a movable top electrode, in order to locally measure electrical or electromechanical properties of the sample. In this case the tips are either coated with a conductive layer or made of a conductive material. The sample itself is provided with a bottom electrode on

which the electroceramic material is deposited or nanofabricated. This geometry allows the application of a voltage to an area of a few hundreds of square nanometers, permitting to probe individual cells of sub-100 nm lateral sizes.

### 4.1. *Electronic Measurements*

Electrical d.c. measurements using the SFM tip as a top electrode are possible in a similar way as normal macroscopic measurements. However, the experiments are very sensitive to the local environment and the reported results are quite contradictory [52, 53]. Our experimental data (Fig. 14), e.g, confirm the space-charge limited type conduction mechanism in EBDW-patterned PZT structures of 100 nm lateral size.

Direct measurements of polarisation hysteresis loops from FIB-milled PZT structures was also achieved [54]. In this case, the charge signal from single submicron capacitors is lower than the shunt capacitance signal of the cantilever. A special correction was employed to get the true polarisation hysteresis loop. The conclusion, however, confirmed previous results [8, 9, 14, 15], according to which there is no size effect in PZT down to a lateral size of 100 nm.

### 4.2. *Piezoresponse Scanning Force Microscopy*

The local polarisation state and the electromechanical properties of ferroelectric thin films and nanostructures can be probed *via* the converse piezoelectric effect using SFM combined with a lock-in technique. This technique is based on the detection of local vibrations of a ferroelectric sample induced by a testing a.c. signal applied between the conductive tip of the SFM and the bottom electrode of the sample [55, 56]. The mechanical oscillations of the sample underneath the tip are transmitted to the cantilever, provided that the contact between tip and sample is firm. This condition is fulfilled when the contact force is dominating over the electrostatic and adhesion forces, i.e. the SFM is in the contact mode of operation with stiff cantilevers. The oscillations of the cantilever are then detected from the global cantilever deflection using a standard lock-in

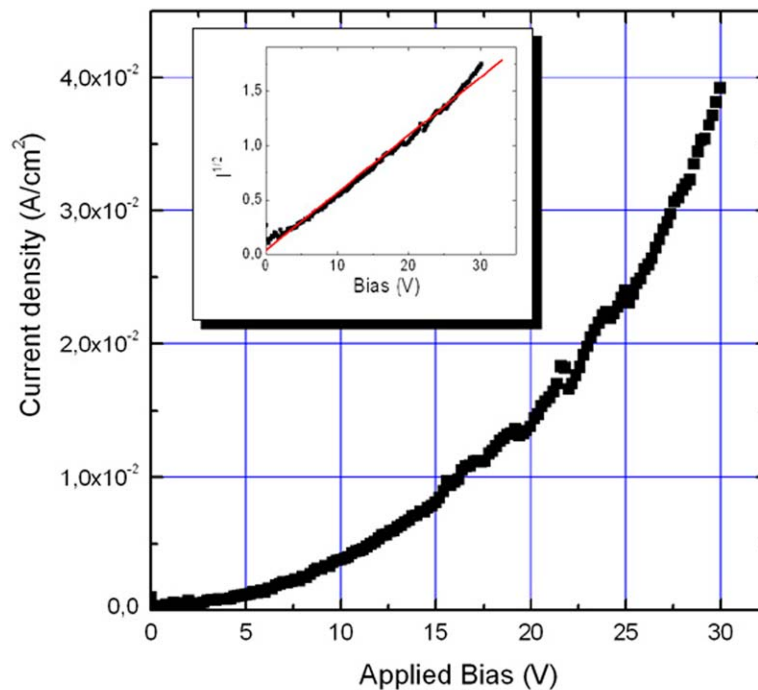


*Fig. 14.* I–V curve of a PZT cell of 100 nm lateral size, measured with a Pt-coated SFM tip consisting of diamond. The positive voltage was applied to the Pt-coated tip serving as the top electrode. The inset shows the same curve replotted into a $I^{1/2}$ *vs.* voltage plot, the straight line corresponding to the linear fit.

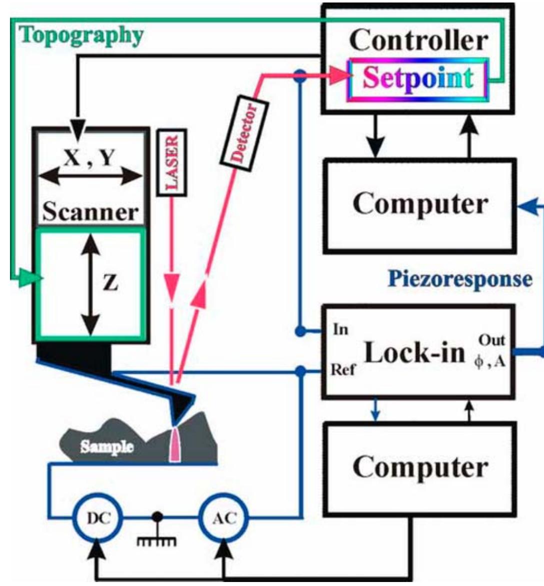


*Fig. 15.* Typical experimental setup for piezoresponse imaging.

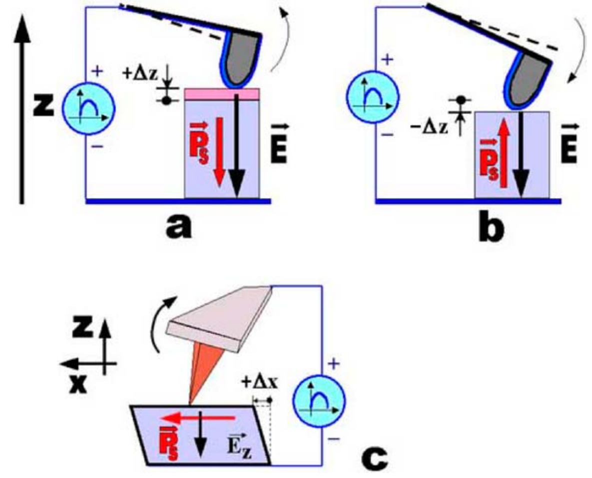


*Fig. 16.* Principle of piezoresponse force microscopy. (a) Piezoelectric expansion when the electric field and the polarization have the same direction. (b) Piezoelectric contraction of the material when the directions of the polarization and of the electric field are opposite. (c) Lateral displacement of the surface due to the induced shear strain.

technique (Fig. 15). Since the first harmonic of the oscillations represents the piezoelectric constant, these vibrations converted into an electrical a.c. signal are further referred to as the piezoresponse signal, or PRS.

The most prominent feature in piezoresponse detection of the polarisation at the surface of an electroceramic material is the strong relation between the piezoelectric coefficient and the spontaneous polarisation. The sign of the piezoelectric coefficient, which determines whether the material expands or contracts, is given by the direction of the spontaneous polarisation with respect to that of the applied electric field. This allows the detection of the direction of the out-of-plane (OP) component of polarisation ($P_z$). Figures 16(a) and (b) illustrate the principle: If the electric field and the polarisation are in the same direction, the material will expand (positive piezoelectric coefficient), otherwise it will contract. The magnitude of the PRS is related to the magnitude of the OP-component of the polarisation. In the general case the relationship between the polarisation $P_z$ and the piezoelectric coefficient $d_{zz}$ along a certain direction $z$ is given by tensorial transformations [18], which sometimes results in a non-univocal relation. However, in several particular cases there is a favourable univocal relationship. One of these cases is that of a material of tetragonal crystal symmetry, for which the shear piezoelectric coefficient is not excessively high compared to the longitudinal piezoelectric coefficient [57].

The above depiction of the processes involved in the detection of the PRS can be described mathematically, in the most simplified way, as follows: The OP-PRS is proportional to the surface displacement $\Delta z$ via a calibration factor $\gamma_{\mathrm{AFM}}$, which is given by the cantilever and the optical detection system of the SFM:

$$OPPRS = \gamma_{\mathrm{AFM}} \Delta z.$$

Assuming a uniform electric field, the surface displacement is

$$\Delta z = \begin{cases} \Delta z^{+} = -d_{zz} V_{AC}, & P_z > 0 \\ \Delta z^{-} = d_{zz} V_{AC}, & P_z < 0 \end{cases}$$

where $V_{AC}$ is the amplitude of the applied voltage.

In a.c. measurements, a negative sign can be interpreted as a phase shift of 180° between the respective physical quantities. In other words, domains with opposite orientations of the polarisation will result in out-of-phase piezoresponse signals. The magnitude of $d_{zz}$ is related to the standard piezoelectric coefficients *via* tensor transformations representing rotations of the piezoelectric tensor. For the simple tetragonal symmetry the final relationship is

$$d_{zz}(\theta) = (d_{31} + d_{15}) \sin^2 \theta \cos \theta + d_{33} \cos^3 \theta,$$

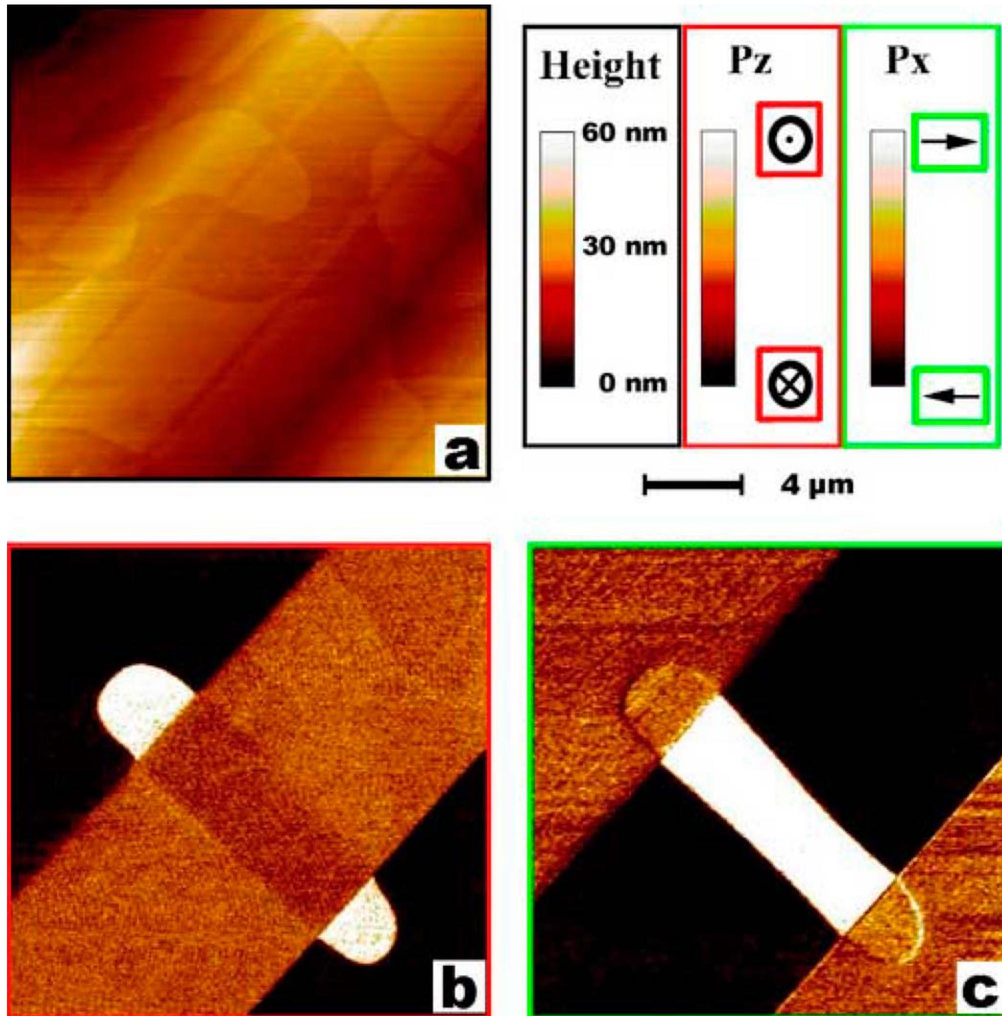


*Fig. 17.* Example of topography and piezoresponse images of the same sample region. (a) Sample topography, (b) OP-PRS and (c) IP-PRS of a barium titanate single crystal exhibiting an $a - c$ lamellar ferroelectric domain structure. (Sample courtesy to Prof. L.M. Eng, Dresden, Germany).

where $\theta$ is the angle between the direction of measurement z and the vector of the spontaneous polarisation. Since all piezoelectric coefficients are related to the magnitude of the spontaneous polarisation[2] [57] it can be concluded that the magnitude of OP-PRS gives an idea of the OP component of the polarisation $P_z = P_S \cos(\theta)$ if the above equation is univocal.

The detection of an in-plane (IP) component of the polarisation vector (parallel to the sample surface) using the converse piezoelectric effect is also possible [58]. The basic principle of this detection consists in the existence of piezoelectric shear deformations (Fig. 16(c)). If the polarisation vector is perpendicular to the electric field, there is no piezoelectric deformation along the field direction, but a shear strain appears in the ferroelectric, leading to displacements of the sample surface parallel to itself, along the polarisation direction. The IP displacements of the surface are transferred *via* friction to the SFM tip as lateral movements. The component of these movements perpendicular to the cantilever axis induces a torsion of the cantilever end, which can be detected using the capability of the SFM to measure the cantilever torsion.

As in the case of detection of the domains with OP polarisation, an a.c. field induces IP oscillations phase shifted by 180° in regions with opposite orientations

of the polarisation. However, due to the complex nature of the friction interaction it is difficult to describe them quantitatively. It should be noted that a shear deformation can be present along both the x-and y-axes, but due to the cantilever geometry, domains having a polarisation along the y-axis can be recorded only by physically rotating the sample by 90°.

Figure 17 shows an example of piezoresponse imaging at the surface of a bulk (001)-oriented barium titanate single crystal. The two PRS images (Figs. 17(b) and (c)) were acquired simultaneously with the sample topography (Fig. 17(a)). The topographic data show the presence of facets making an angle of 0.5°, close to the theoretical value of the tetragonal distortion for barium titanate of 0.6°. Surface steps, about 10 nm in height, are also visible, which have no correlation with the actual ferroelectric domain structure. The images (b) and (c) in Fig. 17 display the OP-PRS and the IP-PRS, respectively, for the same region. The complementary character of the two images is obvoius: Regions with high $P_Z$-contrast (black or white color in image b) exhibit zero $P_X$-contrast (grey color in image c). In other words, a certain point of the surface can have a polarisation either perpendicular or parallel to the surface, in complete agreement with the crystallographic orientation of the sample. However, it should be kept in mind that in order to determine all three components of the vector of polarisation, additional information is required. In the case of a barium titanate single crystal it is sufficient to know the crystallographic orientation of the sample, but this may not be the case for materials with a lower symmetry, or for polycrystalline films.

By definition, ferroelectricity implies that the domains can be switched by an external electric field. In addition to ferroelectric domain imaging, PFM permits the control of ferroelectric domains, i.e. it allows to induce switching by applying a d.c. bias voltage between the tip and the bottom electrode. The most important proof of ferroelectricity is the presence of a piezoelectric hysteresis. The latter is generally recorded using a d.c. bias source connected in series with the a.c. voltage source (cf. Fig. 15). Hysteresis loops are obtained by sweeping the bias voltage and recording the piezoresponse signal while the SFM tip is kept fixed above the desired region of the sample. The result of this procedure is named *in-field* (I-F) hysteresis loop. In addition to this procedure, the d.c. bias may be applied in the form of pulses and the PRS recorded between the pulses, i.e. while no bias is applied to the sample [59]. In this way any electrostatic interaction is avoided. The

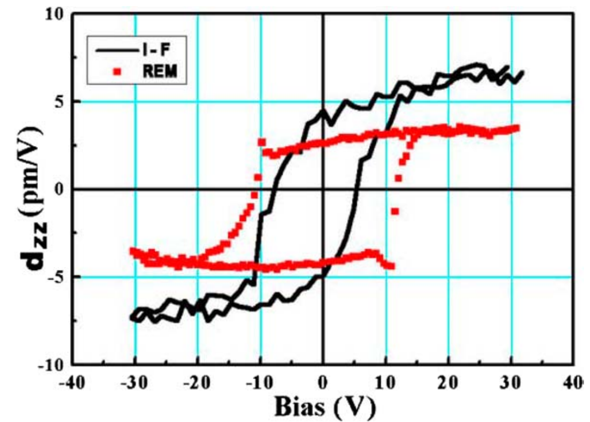


*Fig. 18.* In-field (I-F) and remanent (REM) piezoelectric hysteresis loops of a PZT grain.

resulting hysteresis loop is named *remanent* (REM) loop [59]. It provides additional information on the switching process, on retention and imprint. As an example, Fig. 18 shows an I-F and a REM hysteresis loop recorded from the same PZT (40/60) grain in a 400 nm thick film. Whereas the I-F loop (dark curve) shows a symmetric hysteresis, the REM loop (bright curve) demonstrates that the positive retention value is actually only about 70% of the negative one, and therefore the grain is imprinted. Additionally, if switching of polarisation is achieved using voltage pulses (instead of a continuous voltage), the coercive voltage required for switching is doubled.

## 5. Summary and Outlook

Several non-conventional patterning techniques are available for micro- and nanopatterning of electroceramics. They are based either on top-down or on bottom-up approaches and have successfully been applied to obtain sub-micron ferroelectric nanostructures.

Focussed ion beam patterning is one of the most versatile methods. It has an important advantage—it can pattern features in a well-known and well characterized material (thin film). It has also some drawbacks, which, however, can be minimized by using the method carefully. Electron beam direct writing is an inexpensive method to prepare arrays of sub-100 nm ferroelectric structures. The high resolution and the versatility are unfortunately obscured by the extremely low writing speed which is due to the serial process flow. Nanoimprint lithography is a potential solution

for large area patterning. It has been proven that it works very well in the micron size, but in the submicron range there are still some difficulties which might be overcome with some effort. Nanoimprint has a major advantage over classical lithography methods due to its possibility of patterning structures on non-flat surfaces. This will most probably have a certain impact in optical applications where the feature size is a micron or larger, and where the surface in use is not always flat.

Bottom-up approaches offer the possibility of fabricating ferroelectric structures with lateral sizes of 10–50 nm, well below the sizes accessible by any of the top-down methods. Unfortunately, registration of the structures is still a major problem of all bottom-up approaches, and quite an effort will be necessary to solve this problem. On the positive side, all bottom-up approaches have two considerable advantages, viz. low cost and large area, which make them potentially attractive for large scale fabrication.

The characterization of sub-micron and nanoscale ferroelectrics has been boosted by the development of piezoresponse SFM (PFM). PFM offers an elegant solution to observe and modify ferroelectric domains, to locally measure piezoelectric properties, and along with other scanning probe microscopy methods it can give insight into various phenomena occurring in ferroelectrics at the nanoscale. Due to its extremely simple setup, PFM has become a standard method to characterize ferroelectric materials.

The successful preparation of sub-micron and nanosize ferroelectric structures and the development of appropriate nanoscale measurement methods open a new emerging field, viz. that of *nanoscale ferroelectrics*. Besides new and exciting physics that waits to be revealed, new fields of application are likely to emerge. Nanoscale ferroelectrics may, e.g., have a certain impact in photonics, where tunable photonic band gap materials might open unlimited perspectives, or in MEMS and NEMS, where, for example, mesoscopic and nanosize ferroelectric/piezoelectric wires and tubes might open the possibility of creating active cantilevers or even on-chip scanning tunneling microscopes [60, 61]. In any case, *nanoscale ferroelectrics* will be part of our near future.

## Acknowledgments

This report is based on experimental work performed together with S. Bhattacharyya, S. Chattopadyay, M.-W. Chu, U. Doß, V. Dragoi, W. Erfurth, N. Kurowsky, A. Pignolet, J. Schilling, R. Scholz, I. Szafraniak, A. Visinoiu, and R.B. Wehrspohn, to whom the authors are grateful for their respective contributions. The authors thank J.F. Scott, R. Ramesh, and L.M. Eng for many fruitful discussions. Special thanks are due to U.M. Gösele for initiating investigations on nano-sized ferroelectrics as well as for numerous stimulating discussions and continuous support.

## Notes

1. Here it is assumed that the interaction force depends only on the distance between the tip and the surface.
2. An exception from this rule is barium titanate, for which $d_{33} = 80$ pm/V and $d_{15} = 400$ pm/V.

## References

1. J.F. Scott, *Ferroelectric Memories* (Springer, Berlin, 2000).
2. M.E. Lines and A.M. Glass, *Principles and Applications of Ferroelectrics and Related Materials* (Clarendon Press, Oxford, 1977).
3. Y.G. Wang, W.L. Zhong, and P.L. Zhang, *Phys. Rev. B*, **51**, 5311 (1995).
4. I. Stolichnov, A. Tagantsev, E. Colla, S. Gentil, S. Hiboux, J. Baborowski, P. Muralt, and N. Setter, *J. Appl. Phys.*, **88**, 2154 (2000).
5. S. Bühlmann, B. Dwir, J. Baborowski, and P. Muralt, *Appl. Phys. Lett.*, **80**, 3195 (2002).
6. J.-F. Lin, J.P. Bird, L. Rotkina, and P.A. Benett, *Appl. Phys. Lett.*, **82**, 802 (2003).
7. C.S. Ganpule, A. Stanishevsky, Q. Su, S. Aggarwal, J. Melngaillis, E. Williams, and R. Ramesh, *Appl. Phys. Lett.*, **75**, 409 (1999).
8. C.S. Ganpule, A. Stanishevsky, S. Aggarwal, J. Melngailis, E. Williams, R. Ramesh, V. Joshi, and C.P. de Araujo, *Appl. Phys. Lett.*, **75**, 3874 (1999).
9. V. Nagarajan, A. Roytburd, A. Stanishevsky, S. Prasertchoung, T. Zhao, L. Chen, J. Melngailis, O. Auciello, and R. Ramesh, *Nature Materials*, **2**, 43 (2003).
10. A. Stanishevsky, B. Nagaraj, J. Melngailis, R. Ramesh, L. Khriachtchev, and E. McDaniel, *J. Appl. Phys.*, **92**, 3275 (2002).
11. H.G. Craighead and L.M. Schiavone, *Appl. Phys. Lett.*, **48**, 1748 (1986).
12. J. Lochau, S. Friedrichowski, D. Dumpich, E.F. Wassermann, M. Winter, and M.T. Reetz, *J. Vac. Sci. Technol. B*, **16**, 77 (1998).
13. S. Okamura, K. Mori, T. Tsukamoto, and T. Shiosaki, *Integr. Ferroelectr.*, **18**, 311 (1997).
14. M. Alexe, C. Harnagea, D. Hesse, and U. Gösele, *Appl. Phys. Lett.*, **75**, 1793 (1999).
15. M. Alexe, C. Harnagea, W. Erfurth, D. Hesse, and U. Gösele, *Appl. Phys. A: Mater. Sci. and Processes*, **70**, 247 (2000).
16. D. Damjanovic, *Rep. Prog. Phys.*, **61**, 1267 (1998).

17. C.H. Ahn, T. Tybell, L. Antognazza, K. Char, R.H. Hammond, M.R. Basley, O. Fischer, and J.-M. Triscone, *Science*, **276**, 1100 (1997).
18. C. Harnagea, A. Pignolet, M. Alexe, and D. Hesse, *Integrated Ferrelectrics*, **44**, 113 (2002).
19. C. Harnagea, M. Alexe, D. Hesse, and A. Pignolet, *Appl. Phys. Lett.*, **83**, 338 (2003).
20. M. Alexe, C. Harnagea, D. Hesse, and U. Gösele, *Appl. Phys. Lett.*, **79**, 242 (2001).
21. S.K. Day, J-J. Lee, and P. Alluri, *Jap. J. Appl. Phys., Pt. 2*, **34**, 3142 (1995).
22. J.F. Scott, K. Watanabe, A.J. Hartmann, and R.N. Lamb, *Ferroelectrics*, **225**, 83 (1999).
23. J.F. Scott and M. Dawber, *Appl. Phys. Lett.*, **76**, 3801 (2000).
24. S.Y. Chou, P.R. Krauss, and P.J. Renstrom, *Appl. Phys. Lett.*, **67**, 3114 (1995).
25. S.Y. Chou, P.R. Krauss, and P.J. Renstrom, *J. Vac. Sci. Technol. B*, **14**, 4129 (1996).
26. S.Y. Chou, P.R. Krauss, and P.J. Renstrom, *Science*, **272**, 84 (1996).
27. C. Harnagea, M. Alexe, J. Schilling, R.B. Wehrspohn, D. Hesse, and U. Gösele, *Appl. Phys. Lett.*, **83**, 1827 (2003).
28. R.B. Wehrspohn and J. Schilling, *MRS Bull.*, **26**, 623 (2001).
29. R.J. Jackman, J.L. Wilbur, and G.M. Whitesides, *Science*, **269**, 664 (1995).
30. E. Kim, Y. Xia, and G.M. Whitesides, *Advanced Materials*, **8**, 245 (1996).
31. P.G. Clem, N.L. Jeon, R.G. Nuzzo, and D.A. Payne, *Mater. Res. Soc. Symp. Proc.*, **435**, 521 (1996).
32. M. Sayer, M. Lukacs, T. Olding, G. Pang, L. Zou, and Y. Chen, *Mater. Res. Soc. Symp. Proc.*, **541**, 599 (1999).
33. L. Dellmann, S. Roth, C. Beuret, G.-A. Racine, H. Lorenz, M. Despont, P. Renaud, P. Vettiger, and N.F. De Rooij, *Sensors and Actuators* **A70**, 42 (1998).
34. T. Rosqvist and S. Johansson, *Sensors and Actuators*, **A97–98**, 512 (2002).
35. R.D. Piner, J. Zhu, F. Xu, S. Hong, and C.A. Mirkin, *Science*, **283**, 661 (1999).
36. D.J. Egeleham and M. Cerullo, *Phys. Rev. Lett.*, **64**, 1943 (1990).
37. R.L. Selin, Ch. Ribbat, M. Grundmann, N.N. Ledentsov, and D. Bimberg, *Appl. Phys. Lett.*, **78**, 1207 (2001).
38. H. Fujisawa, K. Morimoto, M. Shimizu, H. Niu, K. Honda, and S. Ohtani, *MRS Symp. Proc.*, **655**, C.C. 10.4.1. (2001).
39. H. Fujisawa, M. Okaniwa, H. Nonomura, M. Shimizu, and H. Niu, *Presented at 15th Int. Symp. Integrated Ferroelectrics (ISIF)* March 9–12, 2003, Colorado Springs, Colorado/USA.
40. K.S. Seol, S. Tomita, K. Takeuchi, T. Miyagawa, T. Katagiri, and Y. Ohki, *Appl. Phys. Lett.*, **81**, 1893 (2002).
41. A. Visinoiu, M. Alexe, and D. Hesse, MPI Halle. Unpublished results (2002).
42. A Seifert, A. Vojta, J.S. Speck, and F.F. Lange, *J. Mater. Res.*, **11**, 1470 (1996).
43. L. Zhao, A.T. Chen, F.F. Lange, and J.S. Speck, *J. Mater. Res.*, **11**, 1325 (1996).
44. R. Waser, T. Schneller, S. Hoffmann-Eifert, and P. Ehrhart, *Integrated Ferroelectrics*, **36**, 3 (2001).
45. A. Roelofs, T. Schneller, K. Szot, and R. Waser, *Nanotechnology*, **14**, 250 (2003).
46. I. Szafraniak, C. Harnagea, R. Scholz, S. Bhattacharyya, D. Hesse, M. Alexe, and U. Gösele, *Appl. Phys. Lett.*, **83**, 2211 (2003).
47. Y. Lin, H. Skaff, T. Emrik, A.D. Dinsmore, and T.P. Russell, *Science*, **299**, 226 (2003).
48. H. Herrig and R. Hempelmann, *Mater. Lett.*, **27**, 287 (1996).
49. S. Bhattacharyya, S. Chattopadhyay, and M. Alexe, *Mater. Res. Soc. Symp. Proc.*, **740**, I.10.3.1. (2003).
50. S. O'Brien, L. Brus, and C.B. Murray, *J. Amer. Chem. Soc.*, **123**, 12085 (2001).
51. G. Binnig, F.C. Quate, and Ch. Gerber, *Phys. Rev. Lett.*, **56**, 930 (1986).
52. H. Fujisawa, M. Shimizu, T. Horiuchi, T. Shiosaki, and K. Matsushige, *Appl. Phys. Lett.*, **71**, 416 (1997).
53. Z. Xie, E.Z. Luo, J.B. Xu, I.H. Wilson, H.B. Peng, L.H. Zhao, and B.R. Zhao, *Appl. Phys. Lett.*, **76**, 1923 (2000).
54. S. Tiedke, T. Schmitz, K. Prume, A. Roelofs, T. Schneller, U. Kall, R. Waser, C.S. Ganpule, V. Nagarajan, A. Stanishevsky, and R. Ramesh, *Appl. Phys. Lett.*, **79**, 3678 (2001).
55. H. Birk, J. Glatz-Reichenbach, L. Jie, E. Schreck, and K. Dransfeld, *J. Vac. Sci. Technol. B*, **9**, 1162 (1991).
56. K. Franke, J. Besold, W. Haessler, and C. Seegebarth, *Surf. Sci.*, **302**, L283 (1994).
57. A.F. Devonshire, *Philos. Mag.* **42**, 1065 (1951). See also A.F. Devonshire, *Philos. Mag.*, **40**, 1040 (1949).
58. M. Abplanalp, L.M. Eng, and P. Günter, *Appl. Phys. A: Mater. Sci. and Processes* **66**, S231 (1998).
59. C. Harnagea, A. Pignolet, M. Alexe, D. Hesse, and U. Gösele, *Appl. Phys. A: Mater. Sci. and Processes*, **70**, 261 (2000).
60. M. Alexe, Y. Luo, I. Szafraniak, R. Wehrspohn, and M. Steinhart, European Patent Application No. 03000969 (2002).
61. Y. Luo, I. Szafraniak, N.D. Zakharov, V. Nagarajan, M. Steinhart, R.B. Wehrspohn, J.H. Wendorff, R. Ramesh, and M. Alexe, *Appl. Phys. Lett.*, **83**, 440 (2003).